http://dx.doi.org/10.5012/bkcs.2012.33.8.2657

Study of the Resonance Structures of the Preionizing Spectrum of Molecular Hydrogen by Phase-Shifted Multichannel Quantum Defect Theory II

Chun-Woo Lee

Department of Chemistry, Ajou University, Woncheon-Dong, Yeongtong-Gu, Suwon 443-749, Korea
E-mail: clee@ajou.ac.kr
Received March 27, 2012, Accepted May 14, 2012

We obtain the general formulation which can handle the rotational preionization spectrum of H_2 in the region above its H_2^+ ionization threshold, $(^2\Sigma_g^+, v^+ = 0, N^+ = 0)$ converging toward its rotationally excited $(v^+ = 0, N^+ = 2)$ limit and perturbed by the vibrationally excited levels $7p\pi$ $v = 1$ and $5p\pi$ $v = 2$. The formulation is based on phase-shifted multichannel quantum-defect theory. With this formulation, resonance structures are analyzed in detail.

Key Words : Phase-shifted MQDT, Overlapping resonances, Preionization of H_2, Interlopers

Introduction

Autoionization spectra frequently show complex overlapping resonances caused by interlopers. Multichannel quantum defect theory (MQDT) is a powerful tool used to model such complex resonances using only a few parameters.[1] However, resonance structures are not transparently identified in its formulation because of its indirect treatment of resonances. To exhibit resonance behaviors transparently, phase-shifted base pairs were introduced to MQDT by Giusti-Suzor and Fano,[2] although their utility has been limited because of the complicated transformations in multi-closed-channel systems.[3] Instead, this phase-shifted version of MQDT has been used to acquire the minimum required MQDT parameters from the observed spectra.[4] For autoionizing series perturbed by interlopers, however, there is no need to perform all the complicated mathematical transformations to identify the resonance structures. Outline resonance structures acquired using physical simplifications hold for such perturbed series. The remaining derivation is normally much simpler, as first introduced by Cooke and Cromer[5] through the use of phase-shifted MQDT. Their treatment was translated into a simple mathematical form by Ueda,[6] whose simple mathematical formulation was extended by us to a system involving 3 closed channels consisting of an interloper that perturbs two interacting autoionizing Rydberg series.[7,8]

Unlike the case of atomic autoionization spectra, application of phase-shifted MQDT to molecular autoionization spectra is rare, with primitive analyses by Giusti-Suzor and Lefebvre-Brion[9] and by us[10] being the only published reports. The phase-shifted MQDT reported in our previous study[10] was developed with an aim to analyze the resonance structures in the photoionization spectrum of H_2 in the region above the threshold of its ionization to $H_2^+(^2\Sigma_g^+, v^+ = 0, N^+ = 0)$, for which there exists an outstanding study using frame transformation MQDT by Jungen and Dill.[11] But, the previous study failed at obtaining the general formulas and only demonstrated the feasibility of the general formulation by using the symbolic operation functionality of MATLAB® to derive formulas on the fly for each energy point. Although the approach of symbolic operation allowed the decomposition of the interlopers' spectrum from the perturbed autoionizing Rydberg spectrum for the system involving 8 channels, it was found to be too time-consuming to be used practically. The formulation that can handle an arbitrary number of interloper series is highly desirable and is achieved in the present study. The obtained general formulation will be described and applied to the rotational preionization of H_2 perturbed by $7p\pi$ $v = 1$ and $5p\pi$ $v = 2$ to analyze the resonance structures.

System

The practical use of MQDT with atomic systems generally involves phase-shifted MQDT beginning directly from either zero sub-matrices or zero diagonal sub-matrices depending on the system.[4] Consider a system involving n channels composed of $n_c - 1$ interlopers belonging to the upper limits, one closed channel converging to the lower limit and perturbed by the interlopers, and one open channel (see Fig. 1). Let the closed channels be indexed 1 to n_c, and the open channels by n. The ionization thresholds I_i, are taken to satisfy $I_{n_c} \geq \cdots \geq I_2 >> I_1 > I_n$. For such systems, the open-open part K^{oo} and the diagonal elements of the closed-closed part K^{cc} of the short-range reactance matrix K can be set to zero by phase renormalization.[6,12] The phase-shifted reactance matrix is given by

$$\tilde{K} = \begin{pmatrix} 0 & \tilde{K}_{12} & \cdots & \tilde{K}_{1n_c} & \tilde{K}_{1n} \\ \tilde{K}_{12} & 0 & \cdots & \tilde{K}_{2n_c} & \tilde{K}_{2n} \\ \vdots & \vdots & \ddots & \vdots & \vdots \\ \tilde{K}_{1n_c} & \tilde{K}_{2n_c} & \cdots & 0 & \tilde{K}_{n_c n} \\ \tilde{K}_{1n} & \tilde{K}_{2n} & \cdots & \tilde{K}_{n_c n} & 0 \end{pmatrix} = \begin{pmatrix} \tilde{K}^{cc} & \tilde{K}^{co} \\ \tilde{K}^{oc} & \tilde{K}^{oo} \end{pmatrix}, \quad (1)$$

where the tilde indicates the phase being shifted. It is convenient to introduce a coupling parameter $\tilde{\xi}_i (i = 1, 2... n_c)$ for the reactance matrix elements $\tilde{K}_{in}^{oc}$ between the open and closed channels. Its square $\tilde{\xi}_i^2$ is related to the spectral width $\tilde{\Gamma}_i$ of the resonance peak of an autoionizing series i by $\tilde{\Gamma}_i = 4\text{Ryd}\tilde{\xi}_i^2/\pi\nu_i^3$,[2] where Ryd denotes the Rydberg constant, and ν_i denotes the effective quantum number defined by $E = I_i - \text{Ryd}/\nu_i^2$ for channel i. $\tilde{W}_i$ denotes $\tilde{\xi}_i^2$:

$$\tilde{W}_i = \tilde{\xi}_i^2 = \tilde{K}_{in}^2 \tag{2}$$

For molecular systems, the frame-transformation version of MQDT is generally used.[13] The reactance matrices used in this version of MQDT are not of the form of Eq. (1). They can be transformed into the form of (1) by shifting the phases of the channel basis wavefunctions by $\mu = [\mu^c \ \mu^o]$ using the formula given in Ref. [14]. For the photoionization spectrum of molecular hydrogen, a lot of interloper series participate in the photoionization. The description of the extension of the previous formulation[10] of MQDT to include arbitrary numbers of interloper series will be presented in the next section after a brief description of the Ueda's formulation.

Photoionization Cross Section

Photoionization cross sections can be calculated from $\sigma = (4\pi^2\alpha\omega/3)|\mathbf{D}|^2$ where ω is the wave-number of an absorbed photon, α is the fine-structure constant, and $\mathbf{D}$ is the transition dipole moment $(\Psi|T|i)$ from the initial state i to the final energy-normalized autoionizing eigenfunction Ψ.[3] In the phase-shifted MQDT, Ψ will be denoted with a tilde as $\tilde{\Psi}$. The formula can be expanded in terms of the real standing-wave channel basis functions in matrix form as:

$$\tilde{\Psi} = \tilde{\Psi}^o \cos\tilde{\delta} - \tilde{\Psi}^c(\tilde{K}^{cc} + \tan\tilde{\beta})^{-1}\tilde{K}^{co}\cos\tilde{\delta} \tag{3}$$

where $\tilde{\Psi}^c$ represents the column vector composed of standing wave closed channel basis functions $\tilde{\Psi}_i$ with indices running from i = 1 to n_c for the system in Figure 1, and $\tilde{\Psi}^o$ is the open channel standing wave channel basis function and is equal to $\tilde{\Psi}_n$. The standing wave channel basis functions $\tilde{\Psi}_i(R, \omega)$ used in this study are defined in Ref. [3], and take the form $\Sigma_j\Phi_j(\omega)[\tilde{f}_j(R)\delta_{ji} - \tilde{g}_j(R)\tilde{K}_{ji}]$ in the outer region. See Ref. [3] for a description of this form, which is different from the one used by Jungen and Dill.[11] $\tilde{\beta}_i$ in (3) denotes phase shifted $\beta_i (\equiv \pi\nu_i)$ by $\pi\mu_i$ *i.e.*, $\tilde{\beta}_i = \pi(\nu_i + \mu_i)$ where ν_i is the effective quantum number defined by $E = I_i - \text{Ryd}/\nu_i^2$ for channel i. The factor $\cos\tilde{\delta}$ in (3), which is equal to $(1+\tilde{\mathbf{K}}^2)^{-1/2}$, is needed to compensate for the energy non-normalized $\tilde{\Psi}_i$ to make $\tilde{\Psi}$ energy-normalized. In the phase-shifted representation, where $\tilde{K}^{oo}$ is null, the background phase shift $\tilde{\delta}_o$ is zero, whereby $\tilde{\delta}$ is equal to the resonance phase shift $\tilde{\delta}_r$.[15] The resonance phase shift $\tilde{\delta}_r$ can be conveniently obtained from the phase of $\det(\tan\tilde{\beta} + \tilde{\kappa}^{cc})$ (see Eq. (14) of Ref. [16]), where the complex reactance matrix $\tilde{\kappa}^{cc}$ denotes $\tilde{K}^{cc} - i\tilde{K}^{co}\tilde{K}^{oc}$.

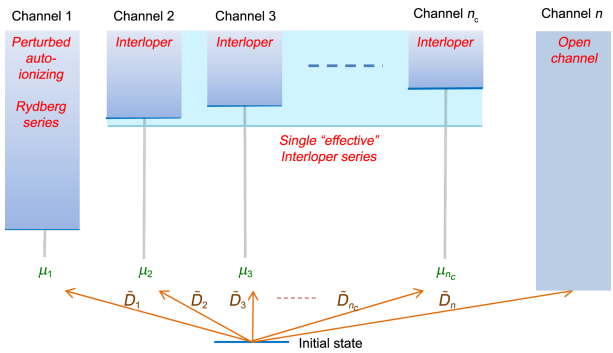

Figure 1. The channel structure of a system comprising one perturbed autoionizing closed channel, arbitrary numbers of interloper channels and one open channel. $\tilde{D}_i$ denotes the transition dipole moment to the channel basis function $\tilde{\Psi}_i$. μ_i denotes the phase shift to make the reactance matrix into the form given by (1).

Closed channels pertaining to higher ionization limits frequently act as interlopers to the autoionizing Rydberg series, providing a broad background to the autoionizing series converging to a lower limit. The influence of a single interloper on the autoionization Rydberg series converging to a lower limit has been examined by Connerade,[17] Cooke and Cromer,[5] and Ueda.[6] An interloper is assumed to be unperturbed by the autoionizing Rydberg series pertaining to a lower limit since its spectral width is normally much broader than that of the autoionizing series with lower limit, so that it ionizes too quickly to be affected by a lower-limit series. According to this physical argument, cross sections can be decoupled into those of an interloper belonging to series 2 and of an autoionizing series 1 perturbed by an interloper:

$$\sigma_{\text{res}} = K\tilde{D}_o^2\frac{(\tilde{\varepsilon}_2+\tilde{q}_2)^2}{\tilde{\varepsilon}_2^2+1}\frac{(\tilde{\varepsilon}_{1\text{eff}}+\tilde{q}_{1\text{eff}})^2}{\tilde{\varepsilon}_{1\text{eff}}^2+1} \equiv \tilde{\sigma}_{\text{interloper}}\frac{(\tilde{\varepsilon}_{1\text{eff}}+\tilde{q}_{1\text{eff}})^2}{\tilde{\varepsilon}_{1\text{eff}}^2+1}, \tag{4}$$

as obtained by Ueda,[6] where K denotes $4\pi^2\alpha\omega/3$, $\tilde{D}_o$ denotes the transition dipole moment to the open channel; and $\tilde{\varepsilon}_2$ and $\tilde{q}_2$ denote the reduced energy and line profile index, respectively, for series 2 acting as an interloper defined by:

$$\tilde{\varepsilon}_2 = \frac{\tan\pi(\nu_2+\mu_2)}{\tilde{W}_2} = \frac{\tan\tilde{\beta}_2}{\tilde{W}_2}$$

$$\tilde{q}_2 = -\frac{\tilde{D}_2}{\tilde{\xi}_2\tilde{D}_o} \tag{5}$$

with $\tilde{\xi}_2$ and $\tilde{W}_2$ defined in (2). $\tilde{D}_i$ denotes the transition dipole moments to the channel basis function $\tilde{\Psi}_i$; $\tilde{\sigma}_{\text{interloper}}$ denotes the autoionizing cross-section of Rydberg series 2 acting as an envelope to the perturbed series; $\tilde{\varepsilon}_{1\text{eff}}$ and $\tilde{q}_{1\text{eff}}$ denote the reduced energy and the line profile index of the perturbed Rydberg series 1, respectively.

The photoionization spectrum of molecular hydrogen considered by Jungen and Dill[11] does not belong to either of the systems mentioned above. More than one interloper series participate in channel coupling to perturb the auto-

ionizing Rydberg series, and the formulation previously developed to separate interlopers' spectra from autoionizing Rydberg series requires extension in order to be able to work with the effects of more than one interloper.

Consider the extension of the interloper spectrum of the previous formulation[10] to an arbitrary number of interloper channels to isolate the interloper's spectrum from the perturbed autoionizing Rydberg series. For an arbitrary number of interloper channels, the notations $\tilde{\varepsilon}_2$ and $\tilde{q}_2$ used in the previous formulation (4) need to be replaced by $\tilde{\varepsilon}_\mathrm{I}$ and $\tilde{q}_\mathrm{I}$, respectively, to indicate that the whole interloper series from 2 to n_c will be treated as a single effective interloper series I. Let us also label the perturbed autoionizing series 1 as p. Then (4) becomes

$$\tilde{\mathbf{D}}^2 = (\tilde{D}^\mathrm{o})^2 \frac{(\tilde{\varepsilon}_\mathrm{I}+\tilde{q}_\mathrm{I})^2}{\tilde{\varepsilon}_\mathrm{I}^2+1} \frac{(\tilde{\varepsilon}_\mathrm{peff}+\tilde{q}_\mathrm{peff})^2}{\tilde{\varepsilon}_\mathrm{peff}^2+1} \tag{6}$$

The form (6) indicates that all interloper series as a whole are treated as a single effective interloper series described by the single reduced energy $\tilde{\varepsilon}_\mathrm{I}$ and line profile index $\tilde{q}_\mathrm{I}$. The form relies on the decomposability of the whole resonance dynamics into the resonance dynamics in the space composed of the interloper channels and the resonance dynamics in the channel pertaining to the lower limit. Resonance dynamics described by the resonance positions and widths are incorporated into the reduced energy parameter $\tilde{\varepsilon}_\mathrm{r}$ defined by $\tan\tilde{\beta}_\mathrm{r}/\tilde{W}_\mathrm{r}$. Since resonance positions and widths are obtainable from the behavior of the phase shift δ_r, the reduced energy and the phase shift are related by $\tilde{\varepsilon}_\mathrm{r} = -\cot\delta_\mathrm{r}$. The decomposability of the resonance dynamics can be formulated into the resonance phase shift. A previous study showed that the resonance phase shift can be obtained from the phase of the determinant of $\tan\tilde{\beta}+\tilde{\kappa}^\mathrm{cc}$:[18] $\left|\tan\tilde{\beta}+\tilde{\kappa}^\mathrm{cc}\right| = C\exp(i\tilde{\delta}_\mathrm{r})$ where the complex reactance matrix $\tilde{\kappa}^\mathrm{cc}$ denotes $\tilde{K}^\mathrm{cc}-i\tilde{K}^\mathrm{co}\tilde{K}^\mathrm{oc}$ with $\Re(\tilde{\kappa}^\mathrm{cc}) = 0$ or $\tilde{K}_{ii} = 0 (i \in \mathrm{Q})$ satisfied for the phase-shifted representation and C denotes the modulus of the determinant. Q denotes the set of closed channels. The bar enclosing a quantity is used to denote the determinant in spite of the possibility of confusion with the notation of the absolute values of complex numbers.

Decomposition can be performed by using the determinant identity $|A| = |B||E-DB^{-1}C|$ for $A = \begin{pmatrix} B & C \\ D & E \end{pmatrix}$.[19] As a preliminary step, $\left|\tan\tilde{\beta}+\tilde{\kappa}^\mathrm{cc}\right|$ is expressed in terms of the reduced energy as $(\Pi_{m\in\mathrm{Q}}\tilde{W}_m)\left|\tilde{\varepsilon}+\rho^\mathrm{cc}\right|$ where the (i,j)th component of the abbreviation ρ^cc of $\tilde{\kappa}_{ij}/(\tilde{\xi}_i\tilde{\xi}_j)$ is given by $(\tilde{K}_{ij}-i\tilde{\xi}_i\cdot\tilde{\xi}_j)/(\tilde{\xi}_i\tilde{\xi}_j) \equiv \tilde{k}_{ij}-i$ for $i\neq j$ and $-i$ for $i=j$. $\tilde{k}_{ij}$ defined by $\tilde{K}_{ij}/(\tilde{K}_{in}\tilde{K}_{jn}) = \tilde{K}_{ij}/(\tilde{\xi}_i\tilde{\xi}_j)$ is the ratio of the direct coupling between closed channels to their indirect coupling *via* open channels. For consistent notation, let us denote $\tilde{\varepsilon}$ as $\tilde{\varepsilon}^\mathrm{cc}$. If the determinant identity is applied, $\left|\tilde{\varepsilon}^\mathrm{cc}+\rho^\mathrm{cc}\right|$ can be decomposed into the terms for the interloper and the perturbed series as follows:

$$\left|\tilde{\varepsilon}^\mathrm{cc}+\rho^\mathrm{cc}\right| = \left|\tilde{\varepsilon}^\mathrm{II}+\rho^\mathrm{II}\right|[\tilde{\varepsilon}_p + \rho_\mathrm{p} - \rho^\mathrm{pI}(\tilde{\varepsilon}^\mathrm{II}+\rho^\mathrm{II})^{-1}\rho^\mathrm{Ip}], \tag{7}$$

with $\tilde{\varepsilon}_{ij}^\mathrm{II}(=\tilde{\varepsilon}_i\delta_{ij})$ and ρ_{ij}^II denoting the elements of sub matrices of the interloper-interloper part whose indices are i and j running for the interloper set $\{\mathrm{I}|i, j = 2, .., n_\mathrm{c}\}$. (The formula for the case of $n_\mathrm{c} = 2$ needs to be treated separately in several occasions in the general formulation for $n_\mathrm{c} \geq 2$. Since (4) can be used for the case of $n_\mathrm{c} = 2$, it is better to assume $n_\mathrm{c} > 2$ without further ado.) The term $\left|\tilde{\varepsilon}^\mathrm{II}+\rho^\mathrm{II}\right|$ can be expressed as $\Im\left|\tilde{\varepsilon}^\mathrm{II}+\rho^\mathrm{II}\right|(\tilde{\varepsilon}_\mathrm{I}-i)$ from which the single reduced energy $\tilde{\varepsilon}_\mathrm{I}$ representing the whole interloper series is obtained. As described in Appendix A, it is obtained as:

$$\tilde{\varepsilon}_\mathrm{I} = \frac{\left|\tilde{\varepsilon}^\mathrm{II}+\tilde{k}^\mathrm{II}\right|}{\sum_{m,n\in\mathrm{I}}\mathrm{cof}_{mn}(\tilde{\varepsilon}^\mathrm{II}+\tilde{k}^\mathrm{II})} = \frac{\left|h^\mathrm{II}\right|}{\sum_{m,n\in\mathrm{I}}\mathrm{cof}_{mn}(h^\mathrm{II})} \tag{8}$$

where cof denotes the cofactor and h^II is introduced to abbreviate $\tilde{\varepsilon}^\mathrm{II}+\tilde{k}^\mathrm{II}$. The roots of $\left|\tilde{\varepsilon}^\mathrm{II}+\tilde{k}^\mathrm{II}\right| = \left|h^\mathrm{II}\right| = 0$ correspond to the resonance positions of the interloper series since they correspond to the most rapidly varying points of $\tilde{\delta}_\mathrm{I}$ defined by $\tilde{\varepsilon}_\mathrm{I} = -\cot\tilde{\delta}_\mathrm{I}$. It may be instructive to rewrite (8) as $\tilde{\varepsilon}_\mathrm{I}^{-1} = \Sigma_{m,n\in\mathrm{I}}[(h^\mathrm{II})^{-1}]_{m,n}$.

Now consider the second term on the right-hand side of (7). The term yields the reduced width $\tilde{W}_\mathrm{peff}$ and energy $\tilde{\varepsilon}_\mathrm{peff}$ of the perturbed autoionizing series 1 from its equivalence to $f_\mathrm{peff}(\tilde{\varepsilon}_\mathrm{peff}-i)$, which is the MQDT version of $E_\mathrm{r}-i\Gamma_\mathrm{r}$. The perturbed reduced width may be decomposed into the unperturbed width $\tilde{W}_\mathrm{p}$ and the enhancement factor f_peff due to perturbation: $\tilde{W}_\mathrm{p}f_\mathrm{peff}$. The derivation described in Appendix B yields:

$$\tilde{W}_\mathrm{peff} = \tilde{W}_\mathrm{p}f_\mathrm{peff} = \tilde{W}_\mathrm{p}\frac{(\tilde{\varepsilon}_\mathrm{I}-k_\mathrm{p\_I})^2}{\tilde{\varepsilon}_\mathrm{I}^2+1} \geq 0$$

$$\tilde{\varepsilon}_\mathrm{peff} = \frac{1}{f_\mathrm{peff}}(\tilde{\varepsilon}_\mathrm{p}-s_\mathrm{p}) \tag{9}$$

where $\tilde{W}_\mathrm{p}$ denotes $\tilde{W}_1 = \tilde{K}_{1n}^2$; $k_\mathrm{p\_I}$ is given by

$$k_\mathrm{p\_I} = -\frac{\sum_{j\in\mathrm{I}}\mathrm{cof}_{jp}(h^\mathrm{cc})}{\sum_{j,k\in\mathrm{I}}\mathrm{cof}_{jk}(h^\mathrm{II})} \tag{10}$$

and s_p is obtained as

$$s_\mathrm{p} = \frac{\sum_{j\in\mathrm{I}}\left\{\left[\left|h^\mathrm{II} \underset{j}{\leftarrow} \tilde{k}^\mathrm{Ip}\right|\tilde{k}_{1j} - \sum_{m,n\in\mathrm{I}}\mathrm{cof}_{m,n}(h^\mathrm{II} \underset{j}{\leftarrow} \tilde{k}^\mathrm{Ip})\right]\tilde{\varepsilon}_\mathrm{I}\right\}}{\left[\sum_{m,n\in\mathrm{I}}\mathrm{cof}_{mn}(h^\mathrm{II})\right](\tilde{\varepsilon}_i^2+1)} \tag{11}$$

where h^cc and h^II denote $\tilde{\varepsilon}^\mathrm{cc}+\tilde{k}^\mathrm{cc}$ and $\tilde{\varepsilon}^\mathrm{II}+\tilde{k}^\mathrm{II}$, respectively, and the notation $h^\mathrm{II} \underset{j}{\leftarrow} \tilde{k}^\mathrm{Ip}$ denotes the matrix h^II whose j^th column is replaced by the column vector $\tilde{k}^\mathrm{Ip}$. (The i^th component of $\tilde{k}^\mathrm{Ip}$ is $\tilde{k}_{i1}$.) From (9), the spectral reduced width $\tilde{W}_\mathrm{peff}$ of the perturbed autoionizing series is zero at the point satisfying $\tilde{\varepsilon}_\mathrm{I} = k_\mathrm{p\_I}$, and can be broadened up to $\tilde{W}_\mathrm{p}(k_\mathrm{p\_I}^2+1)$ at $\tilde{\varepsilon}_\mathrm{I} = -1/k_\mathrm{p\_I}$.

Cross Section Formula. From the formula of the physical wavefunction given by[3]

$$\tilde{\mathbf{\Psi}} = \tilde{\Psi}^{\mathrm{o}}\cos\tilde{\delta}_{\mathrm{r}} + \tilde{\Psi}^{\mathrm{c}}\cos\tilde{\beta}\tilde{Z}^{\mathrm{c}}$$
$$= \tilde{\Psi}^{\mathrm{o}}\cos\tilde{\delta}_{\mathrm{r}} - \tilde{\Psi}^{\mathrm{c}}(\tan\tilde{\beta} + \tilde{K}^{\mathrm{cc}})^{-1}\tilde{K}^{\mathrm{co}}\cos\tilde{\delta}_{\mathrm{r}} \quad (12)$$

the corresponding transition dipole moment $\tilde{\mathbf{D}}$ is obtained as $[\tilde{D}^{\mathrm{o}} - \tilde{D}^{\mathrm{c}}(\tan\tilde{\beta} + \tilde{K}^{\mathrm{cc}})^{-1}\tilde{K}^{\mathrm{co}}]\cos\tilde{\delta}_{\mathrm{r}}$. Using the analytical formula for the inverse of matrix and abbreviating $|\tan\tilde{\beta} + \tilde{K}^{\mathrm{cc}}|$ as D_{cc}, we have

$$\tilde{\mathbf{D}} = \tilde{D}^{\mathrm{o}}\left[D_{\mathrm{cc}} - \frac{\tilde{D}^{\mathrm{c}}}{\tilde{D}^{\mathrm{o}}}\mathrm{adj}(\tan\tilde{\beta} + \tilde{K}^{\mathrm{cc}})\tilde{K}^{\mathrm{co}}\right]\frac{\cos\tilde{\delta}_{\mathrm{r}}}{D_{\mathrm{cc}}}$$
$$= \tilde{D}^{\mathrm{o}}[D_{\mathrm{cc}} + \tilde{q}^{\mathrm{c}}\tilde{K}^{\mathrm{oc}}\mathrm{adj}(\tan\tilde{\beta} + \tilde{K}^{\mathrm{cc}})\tilde{K}^{\mathrm{co}}]\frac{\cos\tilde{\delta}_{\mathrm{r}}}{D_{\mathrm{cc}}} \quad (13)$$

where the last equality follows from the definition of the line profile index $\tilde{q}^{\mathrm{c}}$ given by $-\tilde{D}^{\mathrm{c}}/(\tilde{D}^{\mathrm{o}}\tilde{\xi}^{\mathrm{c}})$; adj($M$) denotes the adjoint of the matrix M; $\tilde{\delta}_{\mathrm{r}}$ denotes the phase of $\tan\tilde{\beta} + \tilde{\kappa}^{\mathrm{cc}}$ whose formula is given later in (19). The second term inside the bracket of the right-hand side of (13) can be expressed in terms of the reduced energy as follows:

$$[\tilde{q}^{\mathrm{c}}\tilde{K}^{\mathrm{oc}}\mathrm{adj}(\tan\tilde{\beta} + \tilde{K}^{\mathrm{cc}})\tilde{K}^{\mathrm{co}}]_{jk} = \left[\sum_{j,k\in\mathrm{Q}}\tilde{q}_j\,\mathrm{cof}_{jk}(h^{\mathrm{cc}})\right]\prod_{m\in\mathrm{Q}}\tilde{W}_m \quad (14)$$

Substituting (14) into (13) yields

$$\tilde{\mathbf{D}} = \tilde{D}^{\mathrm{o}}[D_{\mathrm{cc}} + \tilde{\mathbf{q}}^{\mathrm{c}}\cdot\mathrm{adj}(h^{\mathrm{cc}})I^{\mathrm{cp}}(\tilde{W}^{\mathrm{c}})^{\mathrm{T}}]\frac{\cos\tilde{\delta}_{\mathrm{r}}}{D_{\mathrm{cc}}} \quad (15)$$

where $\tilde{\mathbf{q}}^{\mathrm{c}}$ is the vector whose i^{th} component is given by $-\tilde{D}_i/(\tilde{D}^{\mathrm{o}}\tilde{\xi}_i)$; I^{cp} is a constant vector of ones and thus adj(h^{cc})I^{cp} is a vector whose m^{th} component is given by $\Sigma_{n\in\mathrm{Q}}\mathrm{cof}_{mn}(h^{\mathrm{cc}})$. The scalar product between these two vectors is obtained as $\Sigma_{m\in\mathrm{Q}}\tilde{q}_m\Sigma_{n\in\mathrm{Q}}\mathrm{cof}_{mn}(h^{\mathrm{cc}})$.

We want to express (13) into a decomposed form given by (6). For that, only formulas for the line profile indices $\tilde{q}_{\mathrm{I}}$ and $\tilde{q}_{\mathrm{peff}}$ need to be derived since the formulas for the reduced energies $\tilde{\varepsilon}_{\mathrm{I}}$ and $\tilde{\varepsilon}_{\mathrm{peff}}$ are already obtained in (8) and (9). After a lengthy derivation described in Appendix C, we have

$$\tilde{q}_{\mathrm{I}} = \frac{\sum_{n\in\mathrm{I}}\left|h^{\mathrm{II}} \leftarrow_n \tilde{q}^{\mathrm{I}}\right|}{\sum_{m,n\in\mathrm{I}}\mathrm{cof}_{mn}(h^{\mathrm{II}})} \quad (16)$$

and

$$f_{\mathrm{peff}}\tilde{q}_{\mathrm{peff}} = \tilde{q}_{\mathrm{p}} + s_{\mathrm{p}}$$
$$+\frac{\left\{\begin{array}{l}\tilde{q}_{\mathrm{p}}[\sum_{n\in\mathrm{Q}}\mathrm{cof}_{\mathrm{p}n}(h^{\mathrm{cc}}) - \sum_{n\in\mathrm{I}}\left|h^{\mathrm{II}} \leftarrow_n \tilde{q}^{\mathrm{I}}\right|] - \tilde{k}^{\mathrm{pI}}\mathrm{adj}(h^{\mathrm{II}})\tilde{k}^{\mathrm{Ip}} \\ + \sum_{m\in\mathrm{I}}\tilde{q}_m\left[\mathrm{cof}_{m\mathrm{p}}(h^{\mathrm{cc}}) - \sum_{n\in\mathrm{I}}(-1)^{m+n}(\tilde{k}^{\mathrm{pI}}_{\mathrm{p}m'})\mathrm{adj}(\mathrm{submat}_{m',n'}(h^{\mathrm{II}}))(\tilde{k}^{\mathrm{Ip}}_{n'\mathrm{p}})\right]\end{array}\right\}}{|h^{\mathrm{II}}| + \sum_{n\in\mathrm{I}}\left|h^{\mathrm{II}} \leftarrow_n \tilde{q}^{\mathrm{I}}\right|} \quad (17)$$

where $\tilde{q}^{\mathrm{I}}$ denotes the sub-vector of $\tilde{q}^{\mathrm{c}}$ restricted to the channel space composed of only interloper series. The prime on the sub-index means that rows/columns with primed indexes are deleted. Accordingly, $\mathrm{submat}_{m',n'}(\tilde{\varepsilon}^{\mathrm{II}} + \tilde{k}^{\mathrm{II}})$ denotes the sub-matrx obtained from the matrix $\tilde{\varepsilon}^{\mathrm{II}} + \tilde{k}^{\mathrm{II}}$ by deleting the m^{th} row and n^{th} column; $\tilde{k}^{\mathrm{Ip}}_{n'\mathrm{p}}$ denotes the column sub-vector obtained from the column vector $\tilde{k}^{\mathrm{Ip}}$ by deleting the n^{th} element; and $\tilde{k}^{\mathrm{pI}}_{\mathrm{p}m'}$ is similarly defined.

Eq. (17) shows that $\tilde{q}_{\mathrm{peff}}$ has a singular point at the zero of f_{peff}. Although $\tilde{q}_{\mathrm{peff}}$ becomes infinity at $\tilde{\varepsilon}_{\mathrm{I}} = k_{\mathrm{p\_I}}$ in which f_{peff} is zero, the maximum value of $(\tilde{\varepsilon}_{\mathrm{peff}} + \tilde{q}_{\mathrm{peff}})^2/(\tilde{\varepsilon}^2_{\mathrm{peff}} + 1)$ given by $\tilde{q}^2_{\mathrm{peff}} + 1$ does not go to infinity but is equal to one. This means that the huge enhancement of the autoionization spectrum in the neighborhood of the singular point of $\tilde{q}_{\mathrm{peff}}$ due to the perturbation by interloper series is completely suppressed at the very singular point. In most cases, this suppression can be ignored since the resonance peak of the perturbed series does not likely lie at (or very close to) the pole.

Spectral Widths. Although spectral width Γ can be obtained from the photoionization spectra from the half-width-half-maximum of resonance peaks, it can be better obtained by using its relation with the time-delay $\tau_{\mathrm{D}} = 2\hbar d\delta/dE$ given by $\Gamma = 4\hbar/\tau_{\mathrm{D}}$.[2] In the phase-shifted MQDT, the phase-shift due to background scattering is zero, and the phase shift purely comes from the resonance scattering. In the previous section, it is denoted as $\tilde{\delta}_{\mathrm{r}}$. Since

$$|\tan\tilde{\beta} + \tilde{\kappa}^{\mathrm{cc}}| = (\prod_{m\in\mathrm{Q}}\tilde{W}_m)\left(|h^{\mathrm{cc}}| - \mathrm{i}\sum_{j,k\in\mathrm{I}}\mathrm{cof}_{jk}(h^{\mathrm{cc}})\right) \quad (18)$$

from (A4), we have

$$\tan\tilde{\delta}_{\mathrm{r}} = -\frac{1}{\tilde{\varepsilon}_{\mathrm{r}}} = -\frac{\sum_{j,k\in\mathrm{Q}}\mathrm{cof}_{jk}(h^{\mathrm{cc}})}{|h^{\mathrm{cc}}|} \quad (19)$$

From the Smith's[20] time-delay formula $\tau_{\mathrm{D}} = 2\hbar d\tilde{\delta}_{\mathrm{r}}/dE$ and utilizing the relation

$$\frac{d|h^{\mathrm{cc}}|}{dE} = \mathrm{tr}\left[\frac{d\tilde{\varepsilon}^{\mathrm{cc}}}{dE}\mathrm{adj}(h^{\mathrm{cc}})\right] \quad (20)$$

obtained from the well-known identity $d|xI - A|/dx = \mathrm{tr}[\mathrm{adj}(xI - A)]$,[21] we obtain

$$\tau_{\mathrm{D}} = 2\hbar\frac{\sum_{i\in\mathrm{Q}}\left\{\begin{array}{c}\mathrm{cof}_{ii}(h^{\mathrm{cc}})\sum_{j,k\in\mathrm{Q}}\mathrm{cof}_{jk}(h^{\mathrm{cc}}) - |h^{\mathrm{cc}}| \\ \times\sum_{j,k\in\mathrm{Q},\,\neq\mathrm{i}}[(-1)^{j+k+st(i-j)+st(i-k)}|\mathrm{submat}_{i'j',i'k'}(h^{\mathrm{cc}})|]\end{array}\right\}\frac{d\tilde{\varepsilon}_i}{dE}}{|h^{\mathrm{cc}}|^2 + \left[\sum_{j,k\in\mathrm{Q}}\mathrm{cof}_{jk}(h^{\mathrm{cc}})\right]^2} \quad (21)$$

where $st(t)$ is the step function defined by 0 for $t < 0$ and 1 for $t > 0$. Eq. (21) indicates that the time delay is given as an incoherent sum of the time delays for all closed-series i as

$$\tau_{\mathrm{D}} = \Sigma_{i\in\mathrm{Q}}\tau_{\mathrm{D}i\mathrm{eff}}. \quad (22)$$

Usually, $d\tilde{\varepsilon}_1/dE \equiv d\tilde{\varepsilon}_p/dE >> d\tilde{\varepsilon}_i/dE$ $(i = 2,...)$. Therefore, the time delay is usually approximated with the first term in the summation on the right-hand side of (21): $\tau_D \approx \tau_{Dleff} \equiv \tau_{Dpeff}$. Here, all the terms in (22) will be retained. The first term τ_{Dpeff} can be simplified further and is entitled to a further treatment.

$$\tau_{Dpeff} = 2\hbar \frac{|h^{II}| \sum_{j,k\in Q} \mathrm{cof}_{jk}(h^{cc}) - |h^{cc}| \sum_{j,k\in I} \mathrm{cof}_{jk}(h^{II})}{|h^{cc}|^2 + \left[\sum_{j,k\in Q} \mathrm{cof}_{jk}(h^{cc})\right]^2} \frac{d\tilde{\varepsilon}_p}{dE} \quad (23)$$

It is further simplified to[22]

$$\tau_{Dpeff} = \frac{2\hbar}{f_{peff}(\tilde{\varepsilon}_{peff}^2 + 1)} \frac{d\tilde{\varepsilon}_p}{dE} \quad (24)$$

Or, in terms of the time delay $\tau_{Dp} = 2\hbar d\tilde{\delta}_p/dE$ of the isolated autoionizing Rydberg series, (24) becomes

$$\tau_{Dpeff} = \frac{1}{f_{peff}} \frac{\tilde{\varepsilon}_p^2 + 1}{\tilde{\varepsilon}_{peff}^2 + 1} \tau_{Dp} \geq 0$$

(Equality holds at the root of $f_{peff} = 0$.) (25)

with τ_{Dp} given by

$$\tau_{Dp} = \frac{\pi\hbar}{\mathrm{Ryd}} \tilde{W}_p \nu_p^3 \frac{\tilde{\varepsilon}_p^2 + \tilde{W}_p^{-2}}{\tilde{\varepsilon}_p^2 + 1} > 0 \quad (26)$$

where $\tilde{W}_p$ is defined below (9). Eq. (26) is derived from $\tau_D = 2\hbar d\tilde{\delta}_p/dE$ with $\tilde{\varepsilon}_p = -\cot\delta_p = \tan\pi(\nu_p + \mu_p)/\tilde{W}_p$ and $E = I_p - \mathrm{Ryd}/\nu_p^2$. The right-hand side of (25) does not go to infinity at the zero point of f_{peff}. Instead, it becomes zero at the zero point of f_{peff} due to f_{peff}^2 from another term $(\tilde{\varepsilon}_{peff}^2 + 1)^{-1}$. If the energy dependence of ν_p^3 is ignored, the maximum and minimum values of τ_{Dp} periodically appear at $\tilde{\varepsilon}_p$ equal to zero and infinity with values $(\pi\hbar/\mathrm{Ryd})\tilde{W}_p^{-1}\nu_p^3$ and $(\pi\hbar/\mathrm{Ryd})\tilde{W}_p\nu_p^3$, respectively. Their ratio is given by $\tilde{W}_p^2$.

The spectral width may be obtained from $\Gamma = 4\hbar/\tau_D$. In contrast to the time delays, spectral widths do not have meaning for all the energy points but only at the (resonance) peaks.

$$\Gamma_{peff} = \Gamma_p f_{peff} \frac{1 + \tilde{\varepsilon}_{peff}^2}{1 + W_p^2 \tilde{\varepsilon}_p^2}\bigg|_{\tilde{\varepsilon}_{peff} = 0}$$

$$\Gamma = \frac{4\hbar}{\tau_D}\bigg|_{|h^{cc}| = 0} \quad (27)$$

where Γ_p denotes $4\hbar/\tau_{Dp}$. Γ in (27) is further simplified into

$$\Gamma = \frac{2\sum_{j,k\in I} \mathrm{cof}_{jk}(h^{cc})}{d|h^{cc}|/dE}\bigg|_{|h^{cc}| = 0} \quad (28)$$

by substituting $|\tilde{\varepsilon}^{cc} + \tilde{k}^{cc}| = |h^{cc}| = 0$ into the derivative of (19) with respect to E. The spectral width Γ_I of an interloper peak can be similarly obtained by replacing h^{cc} in (28) with h^{II}. The denominator of (28) can be calculated using (20).

Application to the H_2

The resonance structure of the preionization spectrum[23] of H_2 in the region above its H_2^+ ionization threshold, ($^2\Sigma_g^+$, $v^+ = 0$, $N^+ = 0$), is complicated due to perturbation by the vibrationally excited levels $7p\pi$ $v = 1$ and $5p\pi$ $v = 2$. This spectrum was studied by Jungen and Dill,[11] whose study remains one of the most accurate and extensive despite there being many subsequent relevant studies on hydrogen molecules.[24]

This system was chosen for the development of the phase-shifted formulation of MQDT in the previous study.[10] Unlike the expectation that two interloper series can describe the two interloper peaks assigned to $7p\pi$ $v = 1$ and $5p\pi$ $v = 2$, at least 12 channels are needed for the reproduction of the experimental data without discernible difference from the 22 channel calculation, which is regarded as a full calculation. The formulation in the previous study, however, was limited to the system composed of 1 open, 2 interloper, and 1 autoionizing Rydberg channels, and thus could not handle the spectrum properly. The previous study only demonstrated the feasibility of the general formulation by using the symbolic operation functionality of MATLAB® to derive formulas on the fly for each energy point. Although the approach of symbolic operation allowed the decomposition of the interlopers' spectrum from the perturbed autoionizing Rydberg spectrum for the system involving 8 channels, it was found to be too time-consuming to be used practically.

Since a formulation that can handle the arbitrary number of interloper series is now attained in the previous section, let us apply it to the preionization spectrum of H_2. Numerical details are already described in the previous paper[10] and are omitted here. Before starting the analysis of the resonance structures in the spectrum of H_2, let us first describe the interesting properties that are satisfied by the QDT parameters for this molecular hydrogen system. [The label i of 22 channels defined in Figure 1 corresponds to the vib-rotational quantum numbers of H_2^+ as follows. The channels for v^+ from 1 to 10 with $N^+ = 0$ correspond to $i = 2, 4, ..., 20$. The channels for v^+ from 0 to 10 with $N^+ = 2$ correspond to $i = 1, 3, ..., 21$ ($\equiv n_c$). The channel $i = 22$ ($\equiv n$), which is open, corresponds to $v^+ = 0$ and $N^+ = 0$. Sometimes this labelling system is not convenient and another labelling system I, p, and o introduced earlier are also used, where I stands for the interloper series, p for the perturbed series by interlopers, and o for the open channel. Channels in I may be indexed from 1 to 20 within I itself.]

One of the interesting behaviors in QDT parameters derives from the isotropic nature of the transition dipole matrix elements $d_\Lambda(R)$ to the npΛ Rydberg series of H_2, *i.e.*, $d_\Sigma = d_\Pi \equiv d$ (= 2.86 a.u.), which indicates that a united atom limit holds in the present system of H_2.[25] In this united atom limit, we have

Table 1. 8 channel phase-shifted QDT parameters. 2-, 3-, … , 22-channel phase-shifted QDT parameters can be found in the supplementary materials

(v^+, N^+)	(0,0)	(0,2)	(1,0)	(1,2)	(2,0)	(2,2)	(3,0)	(3,2)
				I (cm^{-1})				
	124417.3	124591.55	126608.64	126773.71	128672.75	128828.96	130613.86	130761.46
				$\tilde{K}$				
(0,0)	0	-0.4328	-0.0142	0.0799	0.0008	0.008	-0.0007	0.0025
(0,2)	-0.4328	0	0.0905	-0.1179	0.0063	-0.0039	-0.0008	-0.0034
(1,0)	-0.0142	0.0905	0	-0.4901	-0.0174	0.1171	-0.0081	0.0013
(1,2)	0.0799	-0.1179	-0.4901	0	0.1329	-0.1929	-0.0086	0.0062
(2,0)	0.0008	0.0063	-0.0174	0.1329	0	-0.5246	-0.0491	0.1188
(2,2)	0.008	-0.0039	0.1171	-0.1929	-0.5246	0	-0.0347	-0.2748
(3,0)	-0.0007	-0.0008	-0.0081	-0.0086	-0.0491	-0.0347	0	0.6787
(3,2)	0.0025	-0.0034	0.0013	0.0062	0.1188	-0.2748	0.6787	0
				μ				
	-0.0037	0.1212	-0.0059	0.1501	-0.0112	0.1704	-1.1035	0.423
				$\tilde{D}$ (a.u.)				
	0.4645	-0.0976	0.6076	-0.1234	0.6407	-0.1473	-0.4998	-0.1701

$$D_i = d\langle J'M''|J''M''10\rangle \sum_{\Lambda}\left[\langle\Lambda|J''\rangle^{J''}\langle\Lambda|N^+\rangle^{J''}\int dR\frac{\chi_{v''}^{J''}(R)\chi_{v^+}^{N^+}(R)}{\cos\pi\mu_{\Lambda}(R)}\right] \quad (29)$$

Although $\mu_{\Lambda}(R)$ is of a different sign for $\mu = \Sigma$ and Π, its cosine is close to one over the significant range of R in which the value of $\chi_{v''}^{J''}(R)\chi_{v^+}^{N^+}(R)$ is significant. Thus, $\cos\pi\mu_{\Lambda}(R)$ can be treated as constant irrespective of Λ, and the summation term of (29) can be approximated as $\delta_{N^+,J''}$ times the Franck-Condon factor. Subsequently, for the present indexing system of alternative appearance of $N^+ = 0$ and 2 as i increases, the values of D_i alternate which is shown in Table 1. Since $N^+ = 2$ for $i = 1$ and $J'' = 0$ for the initial state of H_2, $\tilde{D}_1$ is close to zero. Subsequently, the value of the line profile index $\tilde{q}_1 = -\tilde{D}_1/(\tilde{D}_n\tilde{K}_{1n})$ for the rotational preionization is close to zero and actually obtained as −0.08, thus yielding a spectrum of window type.

Another interesting property of QDT parameters holds for the coupling between the electronic, rotational, and vibrational motions for the present system. If we examine the behaviors of the reactance matrix, one of the conspicuous features is that coupling between the electronic and rotational motions dominates coupling between the electronic and vibrational motions. This behavior in the channel coupling observed in the reactance matrix K_{ij}, for

$$K_{ij} = K_{N^+v^+,N^{+'}v^{+'}} = \sum_{\Lambda}\langle N^+|\Lambda\rangle^{J''}\langle\tan\pi\mu_{\Lambda}\rangle_{v^+v^{+'}}\langle\Lambda|N^{+'}\rangle^{J''} \quad (30)$$

derives from the behaviors of the short-range quantum defects. The short-range quantum defects for the Born-Oppenheimer (BO) states $|\Sigma R\rangle$ are positive, and those for $|\Pi R\rangle$ are negative, indicating that an electron feels attractive potential in $|\Sigma R\rangle$, repulsive potential in $|\Pi R\rangle$. Because of this behavior, (30) is very small for the same N^+ and $N^{+'}$, and large for different N^+ and $N^{+'}$. Because of this propensity, the ratio of the sums of odd terms to that of even terms of $W_i(=\xi_i^2)$ is much larger than 1. In fact, we have $\Sigma_{i\in\text{odd}}W_i/\Sigma_{i\in\text{even}}W_i = 72.7$ for the reactance matrix before phase renormalization, and 930 for the phase-shifted reactance matrix. Dynamical implications of these properties of K may be explored by partitioning the channels into those belonging to $N^+ = 0$ and 2 blocks, but extensive formulation is needed to furnish meaningful results and will be left for future research.

Resonance Structures in the Interloper Spectrum. The rotational preionization spectrum of H_2 in the region immediately above its H_2^+ ionization threshold, ($^2\Sigma_g^+$, $v^+ = 0$, $N^+ = 0$) is greatly complicated due to the perturbation from the interloper series. In the neighborhood of the interloper resonance peaks, the spectrum is dominated by the interloper spectrum, and the present formulation, which views the spectrum as the product of the unperturbed interloper spectrum and the perturbed rotational preionization series, usually holds. This kind of physical simplification holds if the spectral width of the interloper series is much broader than those of the autoionizing series perturbed by an interloper. If the latter condition is met, electrons in an interloper series autoionize so fast according to the uncertainly principle that they have hardly any time to be perturbed by the lower-limit series. Such an assumption is usually satisfied by the fact that the spectral width decreases as ν^3, as the effective quantum number ν increases and interloper series belonging to the higher limit have smaller ν than that of the lower limit series. For the energy range of interest in the H_2 photoionization spectrum, effective quantum numbers for the rotational preionization series are in the range of 30-39, and the interloper's correspond to 5 and 7. Therefore, the assumption seems to be satisfied, but it is not. Although interloper series have smaller effective quantum numbers, their reduced widths become much smaller than that of the lower-limit series because of the large channel

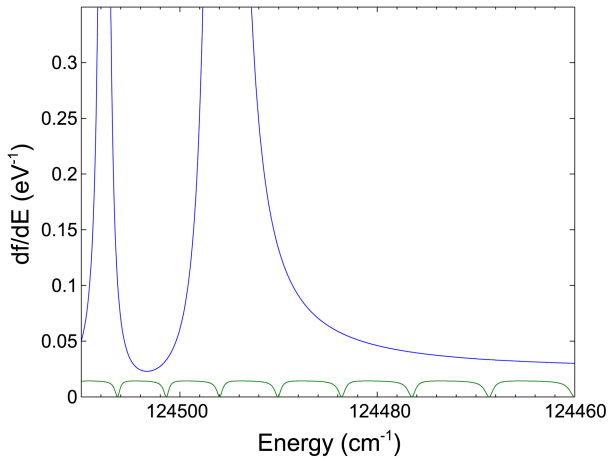

Figure 2. Unperturbed interloper and rotational preionizing series.

coupling between the electronic and rotational motions within the same vibrational quantum number $v^+ = 0$, which is shown in Table 1. Subsequently, the spectral widths Γ of the interloper and the lower-limit series have almost the same magnitudes when the reduced widths are multiplied by $4\text{Ryd}/\pi\nu^3$ [see (26) and (27)].

Although the normal condition for the decomposition into Ueda's formula is not met, Figure 2 shows that the interloper spectrum still dominates the pure rotational autoionization converging to the lower limit. The dominance in magnitude allows us to ignore the perturbation from the lower-limit series to the interloper spectrum and the decomposition into the Ueda's formula may still be physically meaningful for the present system (note that the decomposition can always be performed mathematically without introducing any approximation whether or not such a decomposition is physically meaningful). The reason why the spectrum is dominated by interloper spectrum, with the perturbed rotational preionizing Rydberg series following the envelope it provides, comes from two aspects of channel-channel couplings. In the spectrum of interest, two interloper resonance peaks, 7pπ $v = 1$ and 5pπ $v = 2$, lie close together. In the case of one open channel, the reduced energy $\tilde{\varepsilon}_\text{I}$. defined in (8) for the coupled two series corresponding two resonance peaks, should have a singular point between the peaks. This derives from the fact that the reduced energy for the first peak increases monotonically from $-\infty$ to ∞ *via* 0 at the resonance point in one resonance interval, indicating that it is positive in the interval between two peaks. Similarly, we can see that the reduced energy should be negative in the same interval for the second resonance peak. The only way it can be positive and negative while increasing monotonically in the same interval is that there should be a singular point somewhere in the interval. Then, according to (8) and (16), $\tilde{q}_\text{I}$ also has a singular point at the same energy. Note that two interloper peaks 7pπ $v = 1$ and 5pπ $v = 2$ in the spectrum lie close together, so that the values of $\tilde{q}_\text{I}$ are still large at the two interloper peaks, as shown in Table 2. This contrasts with the values of $\tilde{q}_\text{peff}$ for the rotational pre-ionizing peaks, which is shown in the same table. Note that the ratio of peak

Table 2. The enhancement factors obtained from 22 channel QDT calculation for the interloper and perturbed rotational preionization series, respectively, at the corresponding resonance peaks

$E\|_{\tilde{\varepsilon}_\text{I}=\tilde{q}_\text{I}^{-1}}$ (cm^{-1})	$\tilde{q}_\text{I}$	$\tilde{q}_\text{I}^2+1$
124495.45	-30.44	927.43
12450.72	11.13	124.83
$E\|_{\tilde{\varepsilon}_\text{peff}=\tilde{q}_\text{peff}^{-1}}$ (cm^{-1})	$\tilde{q}_\text{peff}$	$\tilde{q}_\text{peff}^2+1$
124468.10	-0.844	1.713
124475.98	-0.889	1.790
124483.14	-0.973	1.946
124489.61	-1.097	2.204
124496.38	-7.571	58.318
124501.30	-3.286	11.800
124506.01	-2.335	6.451
124510.94	-1.543	3.380
124514.88	-0.619	1.383
124518.58	-0.393	1.154

maxima of the Beutler-Fano terms $(\tilde{\varepsilon}_\text{I}+\tilde{q}_\text{I})^2/(\tilde{\varepsilon}_\text{I}^2+1)$ and $(\tilde{\varepsilon}_\text{peff}+\tilde{q}_\text{peff})^2/(\tilde{\varepsilon}_\text{peff}^2+1)$ in (6) is given by $(\tilde{q}_\text{I}^2+1)/(\tilde{q}_\text{peff}^2+1)$, which is the ratio of the peak maxima of the interloper spectrum to that of the autoionizing Rydberg spectrum. Table 2 shows that the interloper spectrum dominates the autoionizing Rydberg spectrum. Generally, the closer the two interloper peaks lie, the greater the dominance will be.

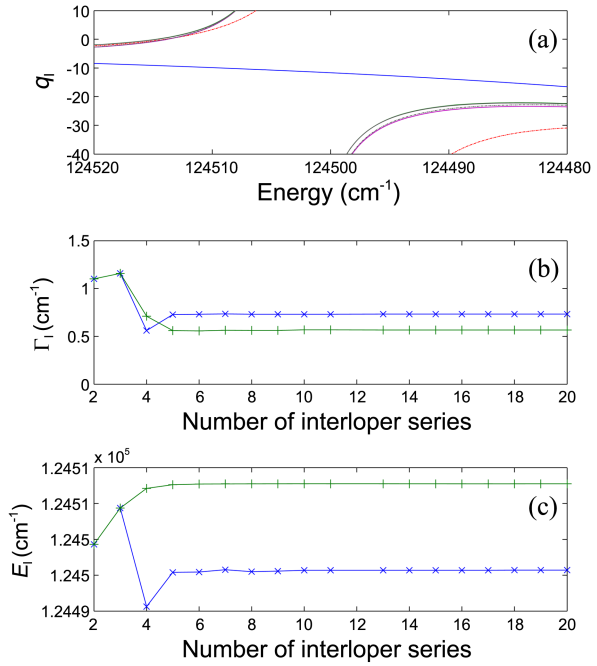

Figure 3. (a) Convergence of the line profile function $\tilde{q}_\text{I}$. Two almost straight lines correspond to 2 and 3 interloper channels. Curves consist of three different groups. One group consists of a single curve corresponding to 4 interloper channels. Another group forming a broad band corresponds to 5-9 interloper channels. The group with a narrow band corresponds to 10-20 interloper channels. (b), (c) The widths and energies of resonance peaks of the interloper spectrum as functions of the number of participating interloper series.

This analysis clearly shows that the spectral behavior in the neighborhood of two interloper peaks 7pπ $v = 1$ and 5pπ $v = 2$ is governed by the interaction of two interloper peaks.

The contributions of interloper channels to the interloper spectrum can be examined from the behaviors of the convergence of the spectral parameter $\tilde{q}_I$, the resonance energies, and the widths of the interloper resonance peaks as functions of the number of participating interloper series. Figure 3 shows that the convergence of the parameters is slow, but the main contribution to the parameters has already reached the number of interloper series as small as 5, which corresponds to $v^+ = 3$. Even contribution up to $v^+ = 3$ amounts to a large number of channel contributions. This indicates that channel-channel coupling among interloper channels is strong.

Channel Coupling Exhibited in the Perturbed Rotational Preionization Spectrum. Let us now consider the rotational preionization spectrum perturbed by interloper series. The perturbation can best be studied by examining the behavior of the line profile function $\tilde{q}_{peff}$. Because of the perturbation, the line profile index of the rotational preionization spectrum is no longer a constant but a function of energy and thus such a phenomenon as q reversal can take place. According to the graph of $\tilde{q}_{peff}$ shown in Figure 4(d), q is negative in most of the range of energy. It becomes positive in a very narrow range of energy. Thus, the spectral shape leans toward the left in most of the range of energy, and the q reversal is not the prominent feature in the spectrum of current interest, although it occurs twice. Instead, spectral enhancement by intensity borrowing from interloper series is the main feature in Figure 4(c), which shows two curves: one is the perturbed rotational preionization spectrum given by $2h\nu(\tilde{\varepsilon}_{peff}+\tilde{q}_{peff})^2/(\tilde{\varepsilon}_{peff}^2+1)$, and the other is the unperturbed given by $2h\nu(\tilde{\varepsilon}_p+\tilde{q}_p)^2/(\tilde{\varepsilon}_p^2+1)$. Spectral enhancement, described by the factor $\tilde{q}_{peff}^2+1$, is caused by the presence of two singular points at $\tilde{\varepsilon}_I = k_{p\_I}$ in which f_{peff} is zero. Figure 4(c) shows that not only spectral enhancement takes place, but also diminishment by the channel coupling with the interloper series occurs. This is caused by the interference between two paths: one from p series and the other from the effective interloper series I.

Figure 4(c) shows that this channel coupling is not limited to the neighborhood of the resonance peaks of the interloper series, but is delocalized over the whole energy range of interest, as already noted by Jungen and Dill.[11] Such nonlocal nature of channel coupling is clearly displayed in Figure 4(d), in which differences in the q values in the perturbed and unperturbed series persist over the entire range of energy. The large nonlocal nature of channel coupling implies that channel coupling takes place at a shorter-range comparing to other cases.

Let us consider the effect of channel coupling on the spectral width Γ of the rotational preionization, which are related to the time delays τ_D by $\Gamma = 4\hbar/\tau_D$. As stated earlier,

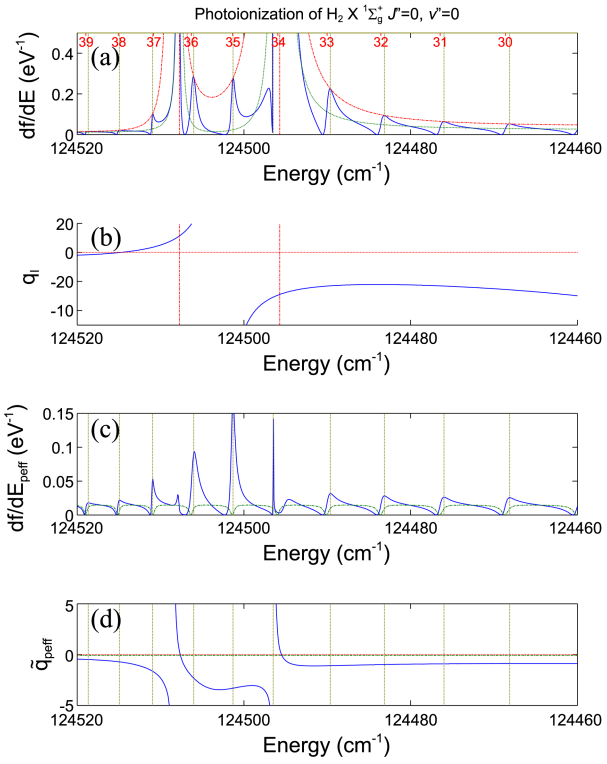

Figure 4. Preionization spectrum obtained by 12 channel QDT calculation. (a) The oscillator strength spectrum is drawn with a solid line, that of the interlopers composed of 10 closed and one open channels with a dashed line and $(df/dE)_{max}$ with a dashed-dot line. The positions of the resonance peak heights of the interloper spectrum are drawn with vertical dashed-dot lines. The positions of the resonance peak maxima of perturbed auto ionizing series are drawn with vertical dotted lines. (b) The graph of the line profile function for the interloper spectrum. (c) The oscillator strength spectrum of the perturbed and unperturbed rotational autoionizing Rydberg series are drawn with solid and dashed-dot lines, respectively. (d) The graph of the perturbed and unperturbed line profile functions $\tilde{q}_{peff}$ and $\tilde{q}_p$ of the rotational autoionizing series are drawn with solid and dotted lines, respectively.

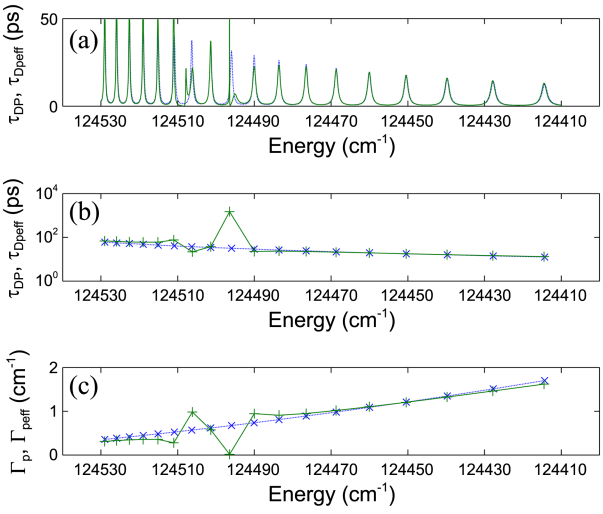

Figure 5. (a) Time delay spectra for the unperturbed and perturbed rotational preionization obtained by 12-channel QDT calculation. (b), (c) Time delays and widths at the resonance peaks of unperturbed and perturbed p series obtained by 22 channel QDT calculation. The dotted line with an x marker corresponds to the unperturbed one and the solid line with + marker to the perturbed one.

time delays have several advantages over the spectral widths. Contrary to the case of spectral widths, the separate contribution of each channel-coupling to the time delays can be examined. Besides that, calculation of time delays can be done for all energies instead of being limited to the positions of resonance as in the case of spectral widths.

Figure 5(a) shows the time delays τ_{Dp} and τ_{Dpeff} in the unperturbed and perturbed rotational preionization, respectively. For the pure rotational preionization, time delay at the peak maximum varies from 12.5 ps to 59.6 ps as the effective quantum number varies from 24.9 to 41.9. The minima in the time delay curve is smaller than the maxima by $\tilde{W}_p^2$, which is 0.035 for the system of interest. Thus, the minimum varies from 0.44 ps to 2.09 ps. Compare the values of time delays with one period of vibration 0.09 ps obtained from $\overline{\omega}_e$ = 2321 cm^{-1} of H_2^+ ($^2\Sigma_g^+$), and one period of rotation 0.23 ps from $\overline{B}_e$ = 30.2 cm^{-1} and $B_eN^+(N^+ + 1) = I\omega^2/2$. Comparison shows that even the minimum time delay in rotational preionization at $\nu_p \approx 25$ is comparable to but a little longer than one period of rotation. Figure 5(b) shows the time delays calculated at the resonance points of the rotational preionization, which correspond to $\tilde{\varepsilon}_p = 0$ for the pure rotational preionization, and $\tilde{\varepsilon}_{peff} = 0$ for the perturbed rotational preionization. According to the figure, the time delay remains close to the unperturbed value, but becomes 1.5 ns at 124496.5 cm^{-1}, which becomes 47 times longer than the unperturbed value by the perturbation of the interloper 5pπ v = 2. In terms of the spectral width, it remains close to the unperturbed value but becomes 0.014 cm^{-1} at 124496.5 cm^{-1}, which is 47 times smaller than the unperturbed value by the perturbation of the interloper 5pπ v = 2 [see Fig. 5(c)]. Thus, unperturbed and perturbed time delays and spectral widths are almost the same in most ranges of energy, except in the neighborhood of two resonance peaks of interloper series. This indicates that the influential range of channel coupling between the auto ionizing Rydberg series p and the interloper series is limited to the neighborhood of resonance peaks of interloper series. The local nature of time delays is related to the derivative with respect to energy. Since the short-range phase shifts are insensitive to the energy variation, they do not contribute to time delays. Thus, the contribution to time delays comes mainly from the long-range region in which Coulomb potential dominates. Because of the dominance of Coulomb potential, the effect of interloper series on the time delays is localized only in the neighborhood of resonance peaks of interloper series.

Resonance Structures of the Spectrum as a Whole. So far, we decomposed the whole preionization spectrum into the interloper spectrum and the rotational preionization spectrum it perturbs, and analyzed the resonance structures of each decomposed spectrum. Since the decomposed spectra are not what is observed, let us consider how those resonance structures identified in the decomposed spectra are manifested in the whole observed spectrum. In this kind of decomposition, it is usually assumed that the resonance structures in the perturbed autoionizing series are not altered

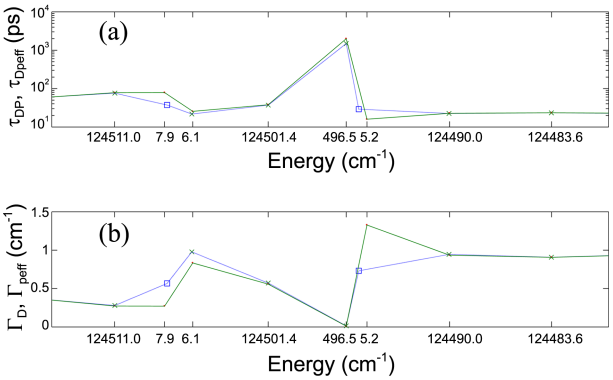

Figure 6. Time delays and spectral widths of the resonance peaks for the decomposed processes and the whole process are obtained by 22 channel QDT calculation. Time delays and widths for the decomposed processes are drawn with the dotted-lines in both (a) and (b) and those for the whole process are drawn with the solid line. The resonance positions for the interloper peaks are marked with a square. Labels for the x-axis denote the resonance energies. To avoid overwriting, only the different last digits are shown for some positions.

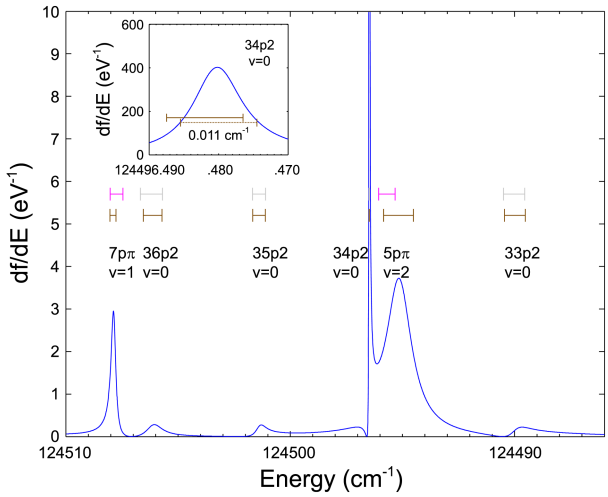

Figure 7. Spectral widths in the neighborhood of two interloper peaks obtained by 22 channel QDT calculation. The lengths of horizontal bars represent the spectral widths and the centers of the bar correspond to the resonance positions. Upper horizontal bars belong to the decomposed spectra and the lower bars to the whole spectrum. The peaks 34p2 v = 0 and 5pπ v = 2 are wrongly assigned in Jungen and Dill.[11] The center of the solid bar in the inlet is drawn at the correct resonance position. The dashed bar has the same length as the solid bar but is shifted to the inside of the peak to demonstrate that it is the width at the half maximum.

in the whole spectrum. This assumption is based on the slow variation of the interloper spectrum. For the present system of interest, the interloper spectrum is composed of two interacting peaks which make the structured background into a type of roller coaster. The resonance structures in the decomposed spectrum may no longer remain unaltered, and are expected to undergo a change in the whole process (6). Figures 6 and 7 show that the difference in resonance structures between the change from the decomposed spectrum and the whole spectrum is only significant in the interloper

spectrum, except for the resonance peak at 124506.1 cm^{-1}. Resonance structures in the perturbed rotational preionization series in the decomposed form are expected to undergo a small change when the whole spectrum is considered, since the channel coupling effect is already included in the perturbed series. The significant change in the resonance structures for the interloper peaks when the whole spectrum is considered may indicate that the resonance structures are actually changed from the interloper spectrum when the rotational preionization series is present. The present formulation properly describes the resonance structures for the perturbed rotational preionization. But for the possible change in resonance structures of the interloper spectrum, no theory is yet available to fully account for the phenomenon.

Results and Discussion

The resonance structure of the preionization spectrum of H_2 in the region immediately above its H_2^+ ionization threshold, with ($^2\Sigma_g^+$, $v^+ = 0$, $N^+ = 0$) converging toward its rotationally excited ($v^+ = 0$, $N^+ = 2$) limit, is complicated, due to the perturbation by the vibrationally excited levels 7pπ $v = 1$ and 5pπ $v = 2$. This system is chosen for the development of the phase-shifted formulation of multichannel quantum defect theory, which decouples the spectrum into the interloper spectrum and the autoionizing Rydberg series perturbed by it. Since at least 12 channels are needed for the reproduction of the experimental data without discernible difference from the 22 channel calculation which is regarded as a full calculation, the formulation that can handle an arbitrary number of interloper channels is needed, and attained in this study. This formulation is applied to the complex preionization spectrum of H_2 to study the resonance structures.

For the present system of interest, the interloper spectrum is composed of interacting two peaks, which make the structured background into the type of roller coaster, for which the spectral widths of the interloper series are almost the same size as those of the autoionizing series perturbed by an interloper, and the usual condition for the decomposition of the spectrum into the interloper's and perturbed spectra is not met. Although the usual condition for the decomposition into Ueda's formula is not met, the interloper spectrum still dominates the perturbed rotational autoionization spectrum in magnitude. This dominance in magnitude gives justification to the application of the formulation developed in this study. Using the decomposed formula, the resonance structures are analyzed in detail. For this spectrum, the q reversal is not the prominent feature, although it actually occurs twice. The q values are negative for most of the spectral range of energy, and the spectral shape leans toward the left in most of the range. Instead, spectral enhancement by intensity borrowing from the interloper series is the main feature, which derives from the interloper-interloper interaction between 7pπ $v = 1$ and 5pπ $v = 2$ peaks. The theory tells us that the closer two interloper peaks lie, the greater the dominance is of the interloper spectrum over the rotational preionizing series.

Time delays and spectral widths perturbed by the interloper series remain almost the same as the unperturbed values in most ranges of energy, except in the neighborhood of two resonance peaks of interloper series. This contrasts to the case of the spectrum of oscillator strength. For the oscillator strength, channel coupling is not limited to the neighborhood of the resonance peaks of the interloper series, but delocalized over the whole energy range of interest. The local nature of time delays is related to the energy insensitiveness of the short-range phase shifts. Thus, the contribution to time delays and spectral widths will be mostly from the long-range region in which Coulomb potential dominates. Because of the dominance of Coulomb potential, the effect of interloper series on the time delays is localized only in the neighborhood of resonance peaks of interloper series.

Time delays of the unperturbed rotational preionization at the maxima of the resonance peaks vary from 12.5 ps to 59.6 ps in the spectral range of energy. However, time delay as long as 1.5 ns is obtained at 124496.5 cm^{-1} by the perturbation of the interloper 5pπ $v = 2$, which is 47 times larger than the unperturbed value.

One interesting problem that has not been dealt with is the more systematic treatment of the dynamic coupling among translational, rotational, and vibrational motions. One way of studying this subject may be to partition the reactance matrix into the $N^+ = 0$ and 2 blocks, and then reformulate all of the formulas. Another subject which has not been dealt with in the present study is the drawing of a map[8,16,22,26] of the photoionization of the whole system whose channel structures are the same as the one for H_2. In order to have a map, the formulas obtained in this study should be more condensed into reduced forms.

Acknowledgments. This study was supported by the Basic Science Research Program through the National Research Foundation of Korea (NRF) funded by the Ministry of Education, Science and Technology (2011-0024808). Support from the Ajou University Research Fellowship of 2011 is also appreciated.

References

1. Aymar, M.; Greene, C. H.; Luc-Koenig, E. *Rev. Mod. Phys.* **1996**, *68*, 1015.
2. Giusti-Suzor, A.; Fano, U. *J. Phys. B* **1984**, *17*, 215.
3. Fano, U.; Rau, A. R. P. *Atomic Collisions and Spectra*; Academic: Orlando, U.S.A., 1986.
4. Kalyar, M. A.; Rafiq, M.; Baig, M. A. *Phys. Rev. A* **2009**, *80*, 052505.
5. Cooke, W. E.; Cromer, C. L. *Phys. Rev. A* **1985**, *32*, 2725.
6. Ueda, K. *Phys. Rev. A* **1987**, *35*, 2484.
7. Lee, C.-W.; Kim, J.; Gim, Y.; Lee, W.-J. *J. Phys. B* **2011**, *44*, 065002.
8. Lee, C.-W. *J. Phys. B* **2011**, *44*, 195005.
9. Giusti-Suzor, A.; Lefebvre-Brion, H. *Phys. Rev. A* **1984**, *30*, 3057.
10. Lee, C.-W. *Bull. Korean Chem. Soc.* **2012**, *33*, 809.
11. Jungen, C.; Dill, D. *J. Chem. Phys.* **1980**, *73*, 3338.

12. Lecomte, J. M. *J. Phys. B* **1987**, *20*, 3645.
13. Greene, C. H.; Jungene, C. *Adv. At. Mol. Phys.* **1985**, *21*, 51.
14. Lee, C.-W.; Kim, J.-H. *Bull. Korean Chem. Soc.* **2002**, *23*, 1560.
15. Lee, C.-W. *Phys. Rev. A* **2002**, *66*, 052704/1.
16. Lee, C.-W. *Bull. Korean Chem. Soc.* **2010**, *31*, 3201.
17. Connerade, J. P. *Proc. R. Soc. London, Ser. A* **1978**, *362*, 361.
18. Lee, C.-W. *Bull. Korean Chem. Soc.* **2009**, *30*, 891.
19. Horn, R. A.; Johnson, C. R. *Matrix Analysis*; Cambridge: Cambridge, U.K., 1985.
20. Smith, F. T. *Phys. Rev.* **1960**, *118*, 349.
21. Cullen, C. G. *Matrices and Linear Transformations*; Dover: New York, 1972.
22. Cho, B.; Lee, C.-W. *Bull. Korean Chem. Soc.* **2010**, *31*, 315.
23. Dehmer, P. M.; Chupka, W. A. *J. Chem. Phys.* **1976**, *65*, 2243.
24. Kirrander, A.; Jungen, C.; Fielding, H. H. *Phys. Chem. Chem. Phys.* **2010**, *12*, 8948.
25. Herzberg, G.; Jungen, C. *Journal of Molecular Spectroscopy* **1972**, *41*, 425.
26. Lee, C.-W. *Bull. Korean Chem. Soc.* **2010**, *31*, 1669.

Appendix A. Formulas for the reduced energy for the effective interloper series

Since the reduced energy $\tilde{\varepsilon}_\mathrm{l}$ for the effective interloper series is defined as $\Im(|\tilde{\varepsilon}^{\mathrm{II}}+\tilde{k}^{\mathrm{II}}|)(\tilde{\varepsilon}_\mathrm{l}-\mathrm{i})$, the separation of $|\tilde{\varepsilon}^{\mathrm{II}}+\tilde{k}^{\mathrm{II}}|$ into the real and imaginary parts is necessary to obtain its formula. From the definition, $\tilde{\varepsilon}^{\mathrm{II}}+\rho^{\mathrm{II}}$ can be written as $\tilde{\varepsilon}^{\mathrm{II}}+\tilde{k}^{\mathrm{II}}-\mathrm{i}$ where $\tilde{\varepsilon}^{\mathrm{II}}+k^{\mathrm{II}}$ is real and where i is a constant matrix of imaginary number i. $\tilde{\varepsilon}^{\mathrm{II}}+k^{\mathrm{II}}-\mathrm{i}$ can be augmented by adding the first row and columns as follows

$$\begin{vmatrix} 1 & 1 & 1 & \cdots & 1 \\ 0 & \tilde{\varepsilon}_2-\mathrm{i} & k_{23}-\mathrm{i} & \cdots & k_{2n_\mathrm{c}}-\mathrm{i} \\ 0 & k_{23}-\mathrm{i} & \tilde{\varepsilon}_3-\mathrm{i} & \cdots & k_{3n_\mathrm{c}}-\mathrm{i} \\ \vdots & \vdots & \vdots & \ddots & \vdots \\ 0 & k_{2n_\mathrm{c}}-\mathrm{i} & k_{3n_\mathrm{c}}-\mathrm{i} & \cdots & \tilde{\varepsilon}_{n_\mathrm{c}}-\mathrm{i} \end{vmatrix} \tag{A1}$$

without changing the value of the determinant. Multiplication of the first row with i and its subtraction from the rows below it transforms the determinant (A1) into the forms in which the real and imaginary parts are separated as

$$\begin{vmatrix} 1 & 1 & 1 & \cdots & 1 \\ \mathrm{i} & \tilde{\varepsilon}_2 & k_{23} & \cdots & k_{2n_\mathrm{c}} \\ \mathrm{i} & k_{23} & \tilde{\varepsilon}_3 & \cdots & k_{3n_\mathrm{c}} \\ \vdots & \vdots & \vdots & \ddots & \vdots \\ \mathrm{i} & k_{2n_\mathrm{c}} & k_{3n_\mathrm{c}} & \cdots & \tilde{\varepsilon}_{n_\mathrm{c}} \end{vmatrix} = \begin{vmatrix} \tilde{\varepsilon}_2 & k_{23} & \cdots & k_{2n_\mathrm{c}} \\ k_{23} & \tilde{\varepsilon}_3 & \cdots & k_{3n_\mathrm{c}} \\ \vdots & \vdots & \ddots & \vdots \\ k_{2n_\mathrm{c}} & k_{3n_\mathrm{c}} & \cdots & \tilde{\varepsilon}_{n_\mathrm{c}} \end{vmatrix} + \mathrm{i} \begin{vmatrix} 0 & 1 & 1 & \cdots & 1 \\ 1 & \tilde{\varepsilon}_2 & k_{23} & \cdots & k_{2n_\mathrm{c}} \\ 1 & k_{23} & \tilde{\varepsilon}_3 & \cdots & k_{3n_\mathrm{c}} \\ \vdots & \vdots & \vdots & \ddots & \vdots \\ 1 & k_{2n_\mathrm{c}} & k_{3n_\mathrm{c}} & \cdots & \tilde{\varepsilon}_{n_\mathrm{c}} \end{vmatrix} \tag{A2}$$

Further reduction of the second term on the right-hand side of (A2) can be obtained by making use of $|A| = |B||E-DB^{-1}C|$ as

$$\begin{aligned} |h^{\mathrm{II}}|[0-I^{\mathrm{pI}}(h^{\mathrm{II}})^{-1}I^{\mathrm{Ip}}] &= -|h^{\mathrm{II}}|I^{\mathrm{pI}}\frac{\mathrm{adj}(h^{\mathrm{II}})}{|h^{\mathrm{II}}|}I^{\mathrm{Ip}} \\ &= -I^{\mathrm{pI}}\mathrm{adj}(h^{\mathrm{II}})I^{\mathrm{Ip}} = -\sum_{m,n\in\mathrm{I}}\mathrm{cof}_{mn}(h^{\mathrm{II}}) \end{aligned} \tag{A3}$$

We thus have

$$|\tilde{\varepsilon}^{\mathrm{II}}+\rho^{\mathrm{II}}| = |h^{\mathrm{II}}| - \mathrm{i}\sum_{m,n\in\mathrm{I}}\mathrm{cof}_{mn}(h^{\mathrm{II}}) = (\sum_{m,n\in\mathrm{I}}\mathrm{cof}_{mn}(h^{\mathrm{II}}))(\tilde{\varepsilon}_\mathrm{l}-\mathrm{i}), \tag{A4}$$

with the reduced energy $\tilde{\varepsilon}_\mathrm{l}$ for the single effective interloper series is obtained as (8).

Appendix B. Derivation of the formulas for f_{peff} and $\tilde{\varepsilon}_{\mathrm{peff}}$

Let us first consider the term contributed by the coupling with the interloper series in (7): $\rho^{\mathrm{pI}}(\tilde{\varepsilon}^{\mathrm{II}}+\rho^{\mathrm{II}})^{-1}\rho^{\mathrm{Ip}}$. To get the formula for the enhancement factor f_{peff} for the reduced spectral width $\tilde{W}_\mathrm{p}$ defined by the imaginary part of the $\tilde{\varepsilon}_\mathrm{p}-\mathrm{i}-\rho^{\mathrm{pI}}(\tilde{\varepsilon}^{\mathrm{II}}+\rho^{\mathrm{II}})^{-1}\rho^{\mathrm{Ip}}$, consider the separation $\rho^{\mathrm{pI}}(\tilde{\varepsilon}^{\mathrm{II}}+\rho^{\mathrm{II}})^{-1}\rho^{\mathrm{Ip}}$ of into the real and imaginary parts. For this purpose, let us rewrite the numerator of $\rho^{\mathrm{pI}}(\tilde{\varepsilon}^{\mathrm{II}}+\rho^{\mathrm{II}})^{-1}\rho^{\mathrm{Ip}}$ as

$$\rho^{\mathrm{pI}}(\tilde{\varepsilon}^{\mathrm{II}}+\rho^{\mathrm{II}})^{-1}\rho^{\mathrm{Ip}} = \frac{\sum_{m\in\mathrm{I}}|\tilde{\varepsilon}^{\mathrm{II}}+\rho^{\mathrm{II}}\underset{n}{\leftarrow}\rho^{\mathrm{Ip}}|\rho_{mp}}{|\tilde{\varepsilon}^{\mathrm{II}}+\rho^{\mathrm{II}}|} \tag{B1}$$

where the notation $\tilde{\varepsilon}^{\mathrm{II}}+\rho^{\mathrm{II}}\underset{n}{\leftarrow}\rho^{\mathrm{Ip}}$ means that the m^{th} column of $\tilde{\varepsilon}^{\mathrm{II}}+\rho^{\mathrm{II}}$ is replaced by ρ_{mp}. The second step of the derivation is the inverse application of the Laplace expansion of determinant. Using the same technique used in Appendix A, we can separate the determinant term $\sum_{j\in\mathrm{I}}|h^{\mathrm{II}}\underset{n}{\leftarrow}k^{\mathrm{Ip}}|\rho_{j\mathrm{p}}$ of the numerator into the real and imaginary parts as follows:

$$\begin{aligned} &\sum_{j\in\mathrm{I}}\Big[|h^{\mathrm{II}}\underset{j}{\leftarrow}k^{\mathrm{Ip}}|+\mathrm{i}\sum_{m,n\in\mathrm{I}}\mathrm{cof}_{m,n}(h^{\mathrm{II}}\underset{j}{\leftarrow}k^{\mathrm{Ip}})\Big](k_{1j}-\mathrm{i}) \\ &= \sum_{j\in\mathrm{I}}|h^{\mathrm{II}}\underset{j}{\leftarrow}k^{\mathrm{Ip}}|k_{1j} - \sum_{j\in\mathrm{I}}\Big(\sum_{m,n\in\mathrm{I}}\mathrm{cof}_{m,n}(h^{\mathrm{II}}\underset{j}{\leftarrow}k^{\mathrm{Ip}})\Big) \\ &-\mathrm{i}\Big[\sum_{j\in\mathrm{I}}|h^{\mathrm{II}}\underset{j}{\leftarrow}k^{\mathrm{Ip}}| + \sum_{j\in\mathrm{I}}\Big(\sum_{m,n\in\mathrm{I}}\mathrm{cof}_{m,n}(h^{\mathrm{II}}\underset{j}{\leftarrow}k^{\mathrm{Ip}})k_{1j}\Big)\Big] \end{aligned} \tag{B2}$$

where h^{II} denotes $\tilde{\varepsilon}^{\mathrm{II}}+\rho^{\mathrm{II}}$. For the sake of convenience, let us abbreviate the four terms of the right-hand side of (B2) as A, Ak, C, Ck so that

$$\sum_{j\in\mathrm{I}}|h^{\mathrm{II}}\underset{j}{\leftarrow}k^{\mathrm{Ip}}|\rho_{j\mathrm{p}} = Ak-C-\mathrm{i}(A+Ck) \tag{B3}$$

Inserting (B3) into (B1) and identifying $\tilde{\varepsilon}_\mathrm{p}-\mathrm{i}-\rho^{\mathrm{pI}}(\tilde{\varepsilon}^{\mathrm{II}}+\rho^{\mathrm{II}})^{-1}\rho^{\mathrm{Ip}}$ with $f_{\mathrm{peff}}(\tilde{\varepsilon}_{\mathrm{peff}}-\mathrm{i})$, we obtain

$$f_{\mathrm{peff}} = 1 + \frac{(Ak-C)\sum_{m,n\in\mathrm{I}}\mathrm{cof}_{mn}(h^{\mathrm{II}}) - (A+Ck)|h^{\mathrm{II}}|}{|h^{\mathrm{II}}|^2 + \Big[\sum_{m,n\in\mathrm{I}}\mathrm{cof}_{mn}(h^{\mathrm{II}})\Big]^2} \tag{B4}$$

and

$$\tilde{\varepsilon}_{\mathrm{peff}} = \frac{1}{f_{\mathrm{peff}}}(\tilde{\varepsilon}_\mathrm{p}-s_\mathrm{p}) \tag{B5}$$

where the shift s_p denotes

$$s_\mathrm{p} = \frac{(Ak-C)|h^{\mathrm{II}}| + (A+Ck)\sum_{m,n\in\mathrm{I}}\mathrm{cof}_{mn}(h^{\mathrm{II}})}{|h^{\mathrm{II}}|^2 + \Big[\sum_{m,n\in\mathrm{I}}\mathrm{cof}_{mn}(h^{\mathrm{II}})\Big]^2} \tag{B6}$$

Study of the time-delay yields the following aesthetically more pleasing expressions for f_{peff} and $\tilde{\varepsilon}_{1\mathrm{eff}}$ as

$$f_{\mathrm{peff}} = \frac{\left|h^{\mathrm{II}}\right| \sum_{j,k\in \mathrm{Q}} \mathrm{cof}_{jk}(h^{\mathrm{cc}}) - \left|h^{\mathrm{cc}}\right| \sum_{j,k\in \mathrm{I}} \mathrm{cof}_{jk}(h^{\mathrm{II}})}{\left|h^{\mathrm{II}}\right|^2 + \left[\sum_{j,k\in \mathrm{I}} \mathrm{cof}_{jk}(h^{\mathrm{II}})\right]^2} \tag{B7}$$

$$\tilde{\varepsilon}_{\mathrm{peff}}^2 + 1 = \frac{\left|h^{\mathrm{cc}}\right|^2 + \left[\sum_{j,k\in \mathrm{Q}} \mathrm{cof}_{jk}(h^{\mathrm{cc}})\right]^2}{\left|h^{\mathrm{II}}\right|^2 + \left[\sum_{j,k\in \mathrm{I}} \mathrm{cof}_{jk}(h^{\mathrm{II}})\right]^2} \tag{B8}$$

For a one-channel system, f_{peff} should be zero once for the effective interloper series, indicating that its numerator should be expressed as a single square term. With fortune, we are able to transform (B7) to (9).

Appendix C. Derivation of $\tilde{q}_{\mathrm{r}}$, $\tilde{q}_{\mathrm{I}}$ and $\tilde{q}_{1\mathrm{eff}}$

For the derivation of the decoupled formula, we need the formula for $\cos\tilde{\delta}_{\mathrm{r}}/D_{\mathrm{cc}}$ which is the last factor of (15). D_{cc} denotes $\tan\tilde{\beta} + \tilde{K}^{\mathrm{cc}}$ and is equal to the real part of $\tan\tilde{\beta} + \tilde{\kappa}^{\mathrm{cc}}$ for the one-open-channel system. It is equal to $C\cos\tilde{\delta}_{\mathrm{r}}$ since $\tan\tilde{\beta} + \tilde{\kappa}^{\mathrm{cc}}$ is $C(\cos\tilde{\delta}_{\mathrm{r}} + \mathrm{i}\sin\tilde{\delta}_{\mathrm{r}})$, yielding $D_{\mathrm{cc}} = C\cos\tilde{\delta}_{\mathrm{r}}$. We thus have

$$\frac{\cos\tilde{\delta}_{\mathrm{r}}}{D_{\mathrm{cc}}} = \frac{1}{C} = \frac{1}{(\tilde{\varepsilon}_{\mathrm{r}}^2+1)^{1/2}\left(\prod_{m\in \mathrm{Q}} \tilde{W}_m\right) \sum_{m,n\in \mathrm{Q}} \mathrm{cof}_{mn}(h^{\mathrm{cc}})} \tag{C1}$$

The second equality of (C1) follows from $\tan\tilde{\beta} + \tilde{\kappa}^{\mathrm{cc}} = \Im(\tan\tilde{\beta} + \tilde{\kappa}^{\mathrm{cc}})(\tilde{\varepsilon}_{\mathrm{r}} - \mathrm{i})$. Substituting (19) and (C1) into (15) yields

$$\tilde{\mathbf{D}} = \tilde{D}^{\mathrm{o}} \frac{\tilde{\varepsilon}_{\mathrm{r}} + \tilde{q}_{\mathrm{r}}}{(\tilde{\varepsilon}_{\mathrm{r}}^2+1)^{1/2}} \tag{C2}$$

with $\tilde{q}_{\mathrm{r}}$ obtained as

$$\tilde{q}_{\mathrm{r}} = \frac{\tilde{\mathbf{q}}^{\mathrm{c}} \cdot \mathrm{adj}^{\mathrm{cc}}(h^{\mathrm{cc}}) I^{\mathrm{cp}}}{\sum_{m,n\in \mathrm{Q}} \mathrm{cof}_{mn}(h^{\mathrm{cc}})} \tag{C3}$$

Let us now consider obtaining the formulas for $\tilde{q}_{\mathrm{I}}$ and $\tilde{q}_{\mathrm{peff}}$ describing the line profiles in the decoupled form (6). The line profile function $\tilde{q}_{\mathrm{I}}$ for the interloper spectrum is obtained by first obtaining the coefficient of $\tilde{\varepsilon}_{\mathrm{p}}$ for the bracketed term of (15) and then subtracting $\tilde{\varepsilon}_{\mathrm{I}}$ from the coefficient. For this purpose, consider the factorizations of the first term D_{cc}

$$D_{\mathrm{cc}} = [\tilde{\varepsilon}_{\mathrm{p}}\left|h^{\mathrm{II}}\right| - \tilde{k}^{\mathrm{pI}} \mathrm{adj}(h^{\mathrm{II}}) \tilde{k}^{\mathrm{Ip}}] \prod_{m\in \mathrm{Q}} \tilde{W}_m \tag{C4}$$

and the second term inside the bracket on the right hand side of (15):

$$\sum_{n\in \mathrm{Q}} [\tilde{q}^{\mathrm{c}} \mathrm{adj}(h^{\mathrm{cc}})]_n = \tilde{q}_{\mathrm{p}} \sum_{n\in \mathrm{Q}} \mathrm{cof}_{\mathrm{p}n}(h^{\mathrm{cc}}) + \sum_{m\in \mathrm{I}} \tilde{q}_m \sum_{n\in \mathrm{Q}} \mathrm{cof}_{mn}(h^{\mathrm{cc}}) \tag{C5}$$

The second term on the right-hand side of (F5) can be further decomposed into

$$\sum_{m\in \mathrm{I}} \tilde{q}_m \sum_{n\in \mathrm{Q}} \mathrm{cof}_{mn}(h^{\mathrm{cc}}) = \sum_{m\in \mathrm{I}} \tilde{q}_m \sum_{n\in \mathrm{Q}} \mathrm{cof}_{m1}(h^{\mathrm{cc}}) + \sum_{m,n\in \mathrm{I}} \tilde{q}_m \mathrm{cof}_{mn}(h^{\mathrm{cc}}) \tag{C6}$$

where $\tilde{\varepsilon}_{\mathrm{p}}$ terms are contained only in the second term on the right hand side of (C6). In order to collect the $\tilde{\varepsilon}_{\mathrm{p}}$ terms, consider the expansion of the term $\mathrm{cof}_{mn}(h^{\mathrm{cc}})$ $m,n \in I$ of the type considered in (7):

$$\mathrm{cof}_{mn}(h^{\mathrm{cc}}) = (-1)^{m+n} \begin{vmatrix} \tilde{\varepsilon}_{\mathrm{p}} & \tilde{k}^{\mathrm{pI}}_{\mathrm{p}n'} \\ \tilde{k}^{\mathrm{Ip}}_{m'\mathrm{p}} & \mathrm{submat}_{m'\mathrm{p}',n'\mathrm{p}'}(h^{\mathrm{cc}}) \end{vmatrix} \tag{C7}$$

$$= (-1)^{m+n}[\tilde{\varepsilon}_{\mathrm{p}}\left|\mathrm{submat}_{m'\mathrm{p}',n'\mathrm{p}'}(h^{\mathrm{cc}})\right| - \tilde{k}^{\mathrm{pI}}_{\mathrm{p}n'} \mathrm{cof}_{m,n}(\mathrm{submat}_{m'\mathrm{p}',n'\mathrm{p}'}(h^{\mathrm{cc}})) \tilde{k}^{\mathrm{Ip}}_{m'\mathrm{p}}]$$

where the prime on the sub-index means that the row/column with primed index is deleted. Substituting (C7) and the relations

$$\sum_{m,n\in \mathrm{I}} (-1)^{m+n} \tilde{q}_m \mathrm{minor}_{m\mathrm{p},n\mathrm{p}}(h^{\mathrm{cc}}) = \sum_{n\in \mathrm{I}} \left| h^{\mathrm{II}} \leftarrow_n \tilde{q}^{\mathrm{I}} \right| \tag{C8}$$

$$\sum_{m\in \mathrm{I}} \tilde{q}_m \mathrm{cof}_{m\mathrm{p}}(h^{\mathrm{cc}}) = \left| h^{\mathrm{cc}} \leftarrow_{\mathrm{I}} \tilde{q}^{\mathrm{I}} \right| \tag{C9}$$

into (C6), we have

$$\tilde{\mathbf{D}} = \tilde{D}^{\mathrm{o}}\left(\prod_{i\in \mathrm{Q}} \tilde{W}_i\right) B \frac{\cos\delta_r}{D_{\mathrm{cc}}} \tag{C10}$$

with B given by

$$\begin{aligned} B = {} & (\tilde{\varepsilon}_{\mathrm{p}} + \tilde{q}_{\mathrm{p}})[\left|h^{\mathrm{II}}\right| + \sum_{n\in \mathrm{I}} \left| h^{\mathrm{II}} \leftarrow_n \tilde{q}^{\mathrm{I}} \right|] \\ & + \tilde{q}_{\mathrm{p}}[\sum_{n\in \mathrm{Q}} \mathrm{cof}_{\mathrm{p}n}(h^{\mathrm{cc}}) - \sum_{n\in \mathrm{I}} \left| h^{\mathrm{II}} \leftarrow_n \tilde{q}^{\mathrm{I}} \right|] - \tilde{k}^{\mathrm{pI}} \mathrm{adj}(h^{\mathrm{II}}) \tilde{k}^{\mathrm{Ip}} \\ & + \sum_{m\in \mathrm{I}} \tilde{q}_m \left[\mathrm{cof}_{m\mathrm{p}}(h^{\mathrm{cc}}) - \sum_{n\in \mathrm{I}} (-1)^{m+n} (\tilde{k}^{\mathrm{pI}}_{\mathrm{p}n'}) \mathrm{adj}(\mathrm{submat}_{m',n'}(h^{\mathrm{cc}}))(h^{\mathrm{II}})(\tilde{k}^{\mathrm{Ip}}_{m'\mathrm{p}})\right] \end{aligned} \tag{C11}$$

Using the formula of $\tilde{\varepsilon}_{\mathrm{I}}$ in (8), the line profile index $\tilde{q}_{\mathrm{I}}$ given in (16) is obtained from the coefficient of $\tilde{\varepsilon}_{\mathrm{p}} + \tilde{q}_{\mathrm{p}}$ term of (C11). Using (B5), (17) is obtained for the last remaining QDT parameter $\tilde{q}_{\mathrm{peff}}$. The denominator of the second term on the right-hand side of (17) is equal to $(\tilde{\varepsilon}_{\mathrm{I}} + \tilde{q}_{\mathrm{I}}) \sum_{m,n\in \mathrm{I}} \mathrm{cof}_{mn}(\tilde{\varepsilon}^{\mathrm{II}} + k^{\mathrm{II}})$.